

**COMPUTATIONAL STUDY
OF THE ACID SITES IN ZEOLITE ZSM-5**

KAIDO SILLAR



Department of Chemistry, University of Tartu, Estonia

Dissertation is accepted for the commencement of the degree of Doctor of Philosophy in Chemistry on June 4, 2004, by the Doctoral Committee of the Department of Chemistry, University of Tartu.

Opponents: Prof. Endel Lippmaa, National Institute of Chemical Physics and Biophysics

Commencement: August 27, 2004, 2 Jakobi St., room 430

© Kaido Sillar, 2004

Tartu Ülikooli Kirjastus
www.tyk.ut.ee
Tellimus nr. 364

CONTENTS

LIST OF ORIGINAL PUBLICATIONS.....	7
1. INTRODUCTION	8
2. BRIEF OVERVIEW OF EXPERIMENTAL IR AND ¹ H NMR MEASUREMENTS OF ZEOLITE ZSM-5	9
2.1 IR spectroscopic studies.....	9
2.2 ¹ H MAS NMR spectroscopic studies.....	10
3. QUANTUM CHEMICAL MODELLING OF HYDROXYL GROUPS IN ZEOLITE ZSM-5	12
4. OVERVIEW OF THE ONIOM METHOD.....	16
5. RESULTS AND DISCUSSION	20
5.1 The test of the ONIOM method.....	20
5.2 Calculation of the properties of acid sites in zeolite ZSM-5.....	28
6. REFERENCES	38
SUMMARY IN ESTONIAN	41
ACKNOWLEDGMENTS	42
PUBLICATIONS	43

LIST OF ORIGINAL PUBLICATIONS

- I K. Sillar, P. Burk, Calculation of the Properties of Acid Sites of the Zeolite ZSM-5 Using ONIOM Method, *J. Mol. Struct. (Theochem)* 589–590 (2002) 281.
- II K. Sillar, P. Burk, Hybrid Quantum Chemical and Density Functional Theory (ONIOM) Study of the Acid Sites in Zeolite ZSM-5, *J. Phys. Chem. B* 108 (2004) 9893.
- III K. Sillar, P. Burk, Computational Study of Vibrational Frequencies of Bridging Hydroxyl Groups in Zeolite ZSM-5, *Chem. Phys. Lett.* 393 (2004) 285.

1. INTRODUCTION

Zeolites are microporous crystalline aluminosilicates with frameworks made of fully linked corner shared SiO_4 and AlO_4 tetrahedra (those tetrahedral atoms are often referred as T-atoms). Insertion of trivalent Al^{3+} in place of tetrahedrally coordinated Si^{4+} creates negative charge on the lattice, which is compensated by extraframework cations. If the charge compensating cations are H^+ , bridged hydroxyl groups, Si-O(H)-Al , are formed, which function as strong Brønsted acid sites. Due to these acid sites, zeolites are solid acids and are used in the petrochemical industry as catalysts. One of those is zeolite ZSM-5 (Zeolite Secony Mobil — five) [1]. The main applications of zeolite ZSM-5 are the catalytic cracking of hydrocarbons (additive in fluid catalytic cracking) and the conversion of methanol to gasoline (MTG process). Also, processes such as the production of ethylbenzene by alkylation of benzene, xylene isomerization and toluene disproportionation run over ZSM-5 containing catalysts [2].

Information about the location of the bridging hydroxyl groups and their distribution over different possible crystallographic positions has great importance in understanding of the catalytic processes deeper. Unfortunately, the experimental techniques that are usually used to determine the structures of solids are not well suited for characterisation of the local structure of the acid sites in zeolites — the X-ray diffraction cannot distinguish Si from Al or locate the acidic protons and therefore the precise location of the bridged hydroxyl groups in zeolite ZSM-5 is not known. Also, because of the low concentration of hydroxyl sites in zeolite ZSM-5 catalysts, even the more sensitive neutron scattering techniques fail.

On the other hand, infrared (IR) and ^1H magic angle spinning nuclear magnetic resonance (MAS NMR) spectroscopy can be used for direct study of the acidic hydroxyl groups in zeolites — different types of hydroxyl groups can be identified and their amount (concentration) can be determined. When the OH groups are in different crystallographic positions in the lattice of zeolites, the differences in local environment around OH groups are reflected in their spectra. But still, because the spectral lines consist of signals from a number of different hydroxyl groups coexisting in zeolites (hydroxyl groups in different geometric environments), the properties of the single acid sites are not sufficiently resolved.

Detailed information about the system at the microscopic level can be obtained from computational modelling. Comparison of the modelled results with the experimental data permits the verification of the underlying model, and if the model appears to be valid, an interpretation of the experimental data can be provided.

In the first part of the current thesis the requirements for computational methods to reproduce the properties of the acid sites of zeolite ZSM-5 are determined. Then the selected method is used to model the structural, energetic and spectroscopic (IR and ^1H NMR) properties of the acid sites of zeolite ZSM-5.

2. BRIEF OVERVIEW OF EXPERIMENTAL IR AND ¹H NMR MEASUREMENTS OF ZEOLITE ZSM-5

2.1 IR spectroscopic studies

Two well-known IR absorption bands are present in the region of the fundamental OH stretch frequencies of zeolite ZSM-5. The sharp peak at 3740 cm⁻¹ corresponds to terminal silanols [3] and somewhat broader peak at 3610 cm⁻¹ (type 1) is assigned to bridging hydroxyl groups [4]. Furthermore, diffuse reflectance IR studies have revealed an additional very broad IR absorption band covering the frequency range from 3600 to 2000 cm⁻¹. This latter band could be assigned to hydroxyl groups (internal silanols or bridging hydroxyl groups) that are influenced by an additional interaction with zeolitic lattice or traces of water adsorbed on strong acid sites [5]. In case of high-silica zeolites and silicalite, the maximum of that latter broad band is at ~3500 cm⁻¹ and the band was assigned to internal silanols, i.e. SiOH groups located in the defect sites of the zeolite framework [6]. On the other hand, for ZSM-5 zeolites with a high crystallinity, the band at ~3250 cm⁻¹ (type 2) predominates. Zholobenko et al. [3] and Brunner et al. [7] have shown that the IR absorption band at ~3250 cm⁻¹ is connected to the bridging hydroxyl groups and thereby, the second type of bridged hydroxyl groups exist in zeolite ZSM-5. This is also confirmed by ¹H NMR measurements [7–9]. Thus, in general, the maximum (or superposition) of broad IR band between 3600 and 3200 cm⁻¹ depends on the pretreatment conditions, zeolite composition, and its structure. The broad bands appear below 2900 cm⁻¹ in the case of strongly hydrogen-bonded water [5,10].

Recently, investigating the heterogeneity of OH groups in zeolite ZSM-5 with high Si/Al ratios, Datka was able to split the IR peak of the first type of bridged hydroxyl groups into five submaxima located between 3606 and 3627 cm⁻¹ [4]. This was achieved by improving the quality of the hydroxyl spectrum, namely by lowering the temperature of measurements to 170 K and exchanging hydrogen atoms in OH groups with deuterium [4]. Furthermore, in steamed zeolite ZSM-5, Datka et al. [11] reported an existence of highly acidic hydroxyl groups characterized by IR band at 3590 cm⁻¹. Splitting of the peak at 3610 cm⁻¹ into several submaxima was explained by the heterogeneity of the OH groups, which in turn was explained by the presence of (SiO)₃-Si-O(H)-Al(OSi)₃ groups of various bridge geometries.

The shape of the IR absorption bands has strong temperature dependence. The signals from both types of bridged hydroxyl groups are clearly resolved in spectra taken at low temperatures. With increasing temperature, the intensity of the broad absorption band of the second type OH groups decreases, while at the same time the band of the free bridging hydroxyl groups broadens and the maximum of that band is shifted toward lower frequencies [3,4].

2.2 ^1H MAS NMR spectroscopic studies

The collection of experimental data from different measurements of ^1H NMR chemical shifts of both types of bridged hydroxyl groups is presented in Table 1.

Table 1. The collection of experimental data from different measurements of ^1H NMR chemical shifts (in ppm) of both types of bridged hydroxyl groups

Type 1	Type 2	Reference
4.3	6.9	8,12
4.2	~ 7	7
4.18 ± 0.05^a	6.1 ± 0.1^b	9
4.3 ± 0.2	6.5 ± 0.5	13, 14
4.2^c	5.4^d	15
3.9	5.9	16
4.0	6.4	17

^afwhm (full-width at half-maximum) = 0.8 ± 0.1 ;

^bfwhm = 2.7 ± 0.3 ; ^cwidth 0.9; ^dwidth 2.9

In general, several ^1H MAS NMR studies have shown existence of two different types of Brønsted acid sites in zeolite ZSM-5, namely free bridging hydroxyl groups (line at ~ 4.2 ppm, type 1) and bridging hydroxyl groups influenced by an additional interaction with the zeolitic framework (line at ~ 7 ppm, type 2) [7–9,12]. The later peak is visible as a broad shoulder on the downfield side of the main peak at 4.2 ppm in many previously measured ^1H MAS NMR spectra of zeolite ZSM-5 [18–22]. This shoulder sharpens into a clearly resolved peak when the temperature is reduced to 123 K [8], which could be explained by a chemical exchange that is frozen at low temperatures [9]. On the basis of the experimental data described above, Freude [9] proposed a model where the hydrogen atom of the second type of bridged hydroxyl group can jump between two or more of the four oxygen atoms around one aluminium atom, and one of these positions is affected by additional electrostatic interaction with other framework oxygen atoms.

It is shown (like in the case of IR spectroscopic measurements) that at room temperature the residual linewidth (about 0.8 ppm) for the signals of the first type of Brønsted acid sites in ^1H MAS NMR spectra of evacuated zeolite catalysts is determined by the distribution width of the isotropic values of the chemical shift, which in turn is explained by structural differences of the bridging hydroxyl groups [12,18,23].

Like in the case of IR spectra, with increasing temperature analogous changes take place also in ^1H NMR spectra: The peak of the second type of bridged hydroxyl group in ^1H NMR spectrum broadens and its intensity decreases with the increase of the peak of the first type of bridged hydroxyl

group [8]. Further increase of the temperature leads to the decrease of intensity and broadening of the one remaining peak characteristic to the first type of bridged hydroxyl groups [8,22]. The changes in spectral shapes with temperature (in the case of both IR and NMR spectra) are completely reversible.

3. QUANTUM CHEMICAL MODELLING OF HYDROXYL GROUPS IN ZEOLITE ZSM-5

Valuable information about energetic, structural and spectroscopic properties of the Brønsted acid sites can be obtained from quantum chemical modelling of hydroxyl groups in zeolites. High-level electron correlation methods and flexible bases sets are needed for quantitative prediction of interaction weaker than covalent bonding (hydrogen bonded systems, intramolecular interactions) or NMR chemical shifts. Zeolites may have several hundred atoms per unit cell, which makes the use of those sophisticated methods computationally very expensive. Modelling active sites of zeolites with relatively small clusters makes it possible to use high-level quantum chemistry methods, but clusters are treated like molecules in the gas phase and therefore they neglect long-range interactions (electrostatic effects) and structure constrains of the periodic solid [24–27]. Consequently, (small) cluster approach cannot discriminate between acid sites in different crystallographic positions or in different frameworks. Full relaxation of clusters may also lead to structures that do not resemble acid sites in real zeolitic lattices [28]. Lattice effects are often implicitly included in calculations by using experimental zeolite structures with only partial geometry optimisation [29–31]. However, Sauer et al. [24] have pointed out that as the local geometry of zeolites acid sites is not precisely known, fixing some geometry parameters may cause artificial strain.

On the other hand, the molecular mechanic studies of zeolites permit the full relaxation of crystal lattice in full unit cell scale and, thus, the long range electrostatic and structure effects are taken into consideration correctly. In context of the properties of acid sites the force field (MM) calculations are mainly focused on studying the distribution of aluminium in the framework of zeolites, i.e. the MM calculation are used to find the preferred locations for acid sites.

Based on classical defect energy calculations Schröder et al. concluded that in the monoclinic structure of zeolite ZSM-5 the T14 site (which corresponds to the T2 site in the orthorhombic structure) is the preferential site for Al/Si substitution [32]. The energy difference between the most and the least favourable T-site for Al substitution is not larger than 5 kcal/mol. These results were obtained with the shell model potential parameterised on empirical data. Nachtigallova et al. [33] carried out lattice energy minimizations and compared the relative stabilities of the structures with aluminium in the 12 distinguishable T-sites of the orthorhombic structure. The results confirm that there are only negligible differences in the energies of the individual structures, however, the difference between the least and most stable structures of 8.6 kcal/mol is somewhat larger than reported by Schröder et al. [32] or Grau-Crespo et al. [34]. The small differences in Al/Si substitution energies indicate that a distribution of Al atoms over broad range of T sites can be expected. Moreover, it has been shown experimentally that Al distribution in ZSM-5 is not controlled

by statistic rules and depends on the conditions of zeolite synthesis [35,36]. Also, ^{27}Al MQ MAS NMR studies have confirmed the existence of at least two non-equivalent aluminium T sites in zeolite ZSM-5 [15,37].

On the basis of cff91_czeo force field [38, 39] calculations, Ricchiardi et al. [40] found that the energy of (Al,H)/Si substitution in the MFI framework is determined more by H position than by the Al position. All the lattice energies of the (Al,H)/Si substitutions in the 96 different positions in monoclinic framework, calculated by Grau-Crespo et al. [34], fall in a range of about 12 kcal/mol. This interval is much wider than the observed for Al/Si replacement, showing the importance of considering the effect of protonation. The most stable acid sites are Al7-O17-Si16 and Al19-O34-Si4, as obtained by Schröder et al. [32]. On the monoclinic-orthorhombic transition, these two sites collapse into one, Al7-O17-Si4. Proton site occupancies were also estimated by considering the acid site formation as a random two-step mechanism in which Al atom is sited first and proton is then bound to one of the adjacent oxygen atoms. This approach suggests Al14-O32-Si18 as the acid site with the largest occurrence. It was also observed that, on average, acid sites with protons located in the large pores of the zeolite are energetically more favourable than those with protons located inside the framework. The last inference is also supported by other molecular mechanics calculations [41] and computational study of large cluster models using semiempirical MNDO method [42].

In a word, force field methods are suited to deal with extended structures built from large unit cells. However, since they are based on effective, classical potentials, they are not able to handle electronic effects (bond breaking or formation) that control the chemical reactivity of zeolites. Also, they are very dependent on data used for force field parameterisation.

The hybrid method approach combines the advantages of quantum mechanical cluster calculations (QM) with the lattice energy minimisations of the periodic solids using molecular mechanical (MM) force fields. The portion of the system in which the reaction is taking place (active site) is modelled by quantum-chemical methods, and the rest of the system is treated with classical force fields. This allows for the inclusion of geometric and electrostatic effects of the rest of the lattice into quantum-chemical models of the (catalytic) reactions at little additional computational cost. Thus, the properties and reactivity of an active site in different environments can be studied.

Sauer et al. have successfully used a combined quantum mechanics/inter-atomic potential function approach (QM-Pot scheme) in investigation of zeolites, including ZSM-5 [25,26]. The approach used describes the Brønsted site by the Hartree-Fock method and a T(O)DZP basis set, while the periodic zeolite framework and the interaction between the active site and the framework are described by a shell model potential parameterized on the same type of ab initio data for cluster models. This method was used to predict the structures of catalysts protonated at different sites. For the orthorhombic form of zeolite ZSM-5 (Si/Al = 95) protonation of the Al7-O17(H)-Si4 site proves more stable

by 2.9 and 1.9 kcal/mol than protonation at the Al12-O24(H)-Si12 or Al2-O6(H)-Si6 sites respectively. To compare the deprotonation energies with values derived from experiments, the systematic deviations due to the error of the Hartree-Fock approximation, the basis set truncation, and the loss of three vibrational degrees of freedom of the acidic proton (the nuclear motion corrections) must be taken into account. Thus, the predicted heat of deprotonation for the Al7-O17(H)-Si4 site was 288 kcal/mol [26]. The latter value was corrected to 295 kcal/mol [24] after finding a correction constant that was obtained by calibration calculations of the deprotonation energies for silanol and methanol, related molecules for which very accurate values are known.

The deprotonation energy obtained by the QM-Pot scheme can be decomposed into the quantum mechanical contribution for the cluster itself and into the long-range contribution. The former reflects the structural constraints imposed on the active site by the framework and the latter the influence of the crystal potential. With increasing cluster size the long-range corrections is found to decrease slowly, while the total QM-Pot energy stays remarkably stable within couple kcal/mol. For example, when embedding a quantum cluster of 14 tetrahedra the long-range corrections is almost as large as when embedding a very small cluster of two tetrahedral only. Only when the QM cluster part includes as many as 28 tetrahedra the long-range correction is significantly reduced (from 20 to 10.5 kcal/mol). This indicates that an increasing share of long-range effects is included in the QM result for the cluster [24,26].

The vibrational frequencies and ^1H NMR chemical shift of the Al7-O17(H)-Si4 site, determined using the QM-Pot scheme, are in reasonable agreement with the experimentally observed values. For the Al2-O6(H)-Si6 site with "internal hydrogen bond" the predicted vibrational frequency is too high (by 280 cm^{-1}) and the predicted ^1H NMR chemical shift too low (by 2.5 ppm) [26]. This can be explained by neglected electron correlation, as it is essential for better description of hydrogen-bonded systems.

The applicability of the ONIOM method (detailed description of this type of hybrid method is given in the next section) to reproduce the properties of the hydrogen-bonded systems and to accurately predict NMR chemical shielding constants is thoroughly investigated by Tschumper et al. [43] and by Karadakov et al. [44], respectively. They have shown that the high-level (QM) part of the system should extend over all atoms that are directly bonded to the atoms of interest. While the ONIOM results for the properties of these additional atoms are likely to be less accurate than those for the atoms of interest, their presence in the high level part reproduces the local environment of the central atoms within the entire molecule and considerably improves the accuracy of the integrated approach.

Roggero et al. [45] have used the ONIOM method to model the isolated hydroxyl group at the silica surface using the octahydrosilasesquioxane cluster. When the high level part included the up to third neighbors of the OH group, $\text{Si}_3\text{O}_3\text{Si}(\text{OH})$, the ONIOM(B3LYP/DZP:HF/3-21G) level of treatment provided

geometries, OH vibrational stretching frequency, NMR isotropic $\delta(^1\text{H})$ and $\delta(^{29}\text{Si})$ chemical shifts and binding energies of NH_3 in excellent agreement with the results computed at the full B3LYP/DPZ level.

By now, only a few theoretical studies of zeolites ZSM-5 and TS-1 have used the ONIOM method [46–49]. Even though they are mainly focused on describing the zeolite-adsorbate complexes, those studies have shown that the lattice effects could be included in the ONIOM method calculations and they have a significant effect on the calculated structural, energetic and spectroscopic properties.

4. OVERVIEW OF THE ONIOM METHOD

The ONIOM (our own n-layered integrated molecular orbital and molecular mechanics) method [50–51], developed by Morokuma and co-workers, is a more general hybrid method, which can combine any number of molecular orbital, as well as molecular mechanics methods. In ONIOM calculation, the molecular system, which is divided into layers or parts, is called the real system. The most important part of the molecule (reaction centre) is called the model system and is described at the highest level of theory. In the two-layered ONIOM method, the total energy of the system is obtained from three independent calculations:

$$E^{\text{ONIOM2}} = E_{\text{model system}}^{\text{high}} + E_{\text{real system}}^{\text{low}} - E_{\text{model system}}^{\text{low}} \quad (1)$$

The ONIOM method can be viewed as an extrapolation scheme. Starting from $E_{\text{model system}}^{\text{low}}$, the extrapolation to the high level calculation ($E_{\text{model system}}^{\text{high}} - E_{\text{model system}}^{\text{low}}$) and the extrapolation to the real system ($E_{\text{real system}}^{\text{low}} - E_{\text{model system}}^{\text{low}}$) are assumed to give an estimate for $E_{\text{real system}}^{\text{high}}$. In case of the three-layered ONIOM method, the ONIOM energy is defined according to equation 2.

$$E^{\text{ONIOM3}} = E_{\text{model system}}^{\text{high}} + E_{\text{middle system}}^{\text{medium}} - E_{\text{model system}}^{\text{medium}} + E_{\text{real system}}^{\text{low}} - E_{\text{middle system}}^{\text{low}} \quad (2)$$

In principle, ONIOM can be used for any number (N) of layers, for which $2N-1$ subcalculations are required.

Thus, if the error D (equation 3) of the extrapolation procedure is *constant* for two different structures (e.g. between reactant and transition state), their relative energy $\Delta E_{\text{real system}}^{\text{high}}$ will be evaluated correctly by using the ONIOM energy ΔE^{ONIOM} .

$$D = E_{\text{real system}}^{\text{high}} - E^{\text{ONIOM}} \quad (3)$$

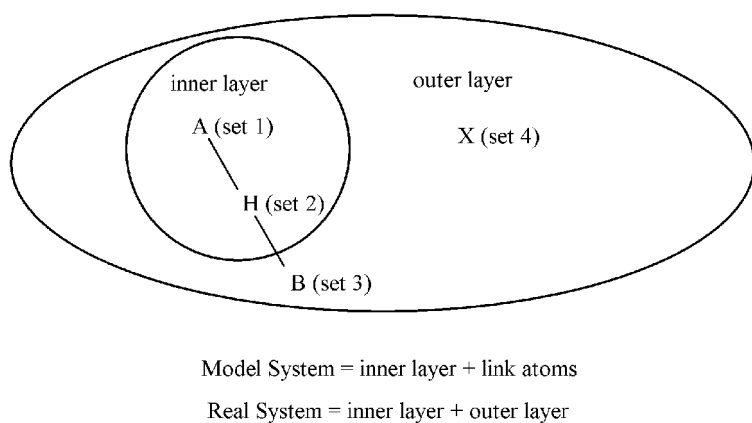


Figure 1. Definition of different atom sets within the ONIOM scheme.

The atoms in the (two-layered) ONIOM scheme can be divided into four sets, each of them with its corresponding coordinates (Figure 1). The atoms present both in the model system and the real system are called set 1 atoms and their coordinates are denoted by \mathbf{R}_1 . The set 2 atoms are the artificially introduced link atoms. The link atoms only occur in the model system because they are used to saturate the dangling bonds resulting from cutting covalent bonds between the model and the real system. The link atom coordinates are described by \mathbf{R}_2 . In the real system they are replaced by the atoms described by \mathbf{R}_3 . Atoms that belong to the outer layer and are not substituted by link atoms are called set 4 atoms with coordinates \mathbf{R}_4 . The geometry of the real system is thus described by \mathbf{R}_1 , \mathbf{R}_3 , and \mathbf{R}_4 and they are independent coordinates for the ONIOM energy:

$$E^{ONIOM} = E^{ONIOM}(\mathbf{R}_1, \mathbf{R}_3, \mathbf{R}_4) \quad (4)$$

In order to generate the model system, described by \mathbf{R}_1 and the link atoms \mathbf{R}_2 , the \mathbf{R}_2 is defined as a function of \mathbf{R}_1 and \mathbf{R}_3 :

$$\mathbf{R}_2 = f(\mathbf{R}_1, \mathbf{R}_3) \quad (5)$$

The explicit functional form of the \mathbf{R}_2 dependency can be chosen arbitrarily. However, considering the fact that the link atoms are introduced to mimic the corresponding covalent bonds of the real system, they should follow the movement of the atoms they replace. Therefore the following coupling scheme is adopted. If atom A belongs to set 1 and atom B belongs to set 3, the set 2 link atom (symbolized by H in Figure 1) is placed onto the bond axis A–B. In terms of the internal coordinates the same bond angles and dihedral angles for set 2 as

for set 3 are chosen. Therefore, in the model system calculations the link atoms are always aligned along the bond vectors of the real system. For the exact position \mathbf{r}_2 of a single link atom along an A–B bond ($\mathbf{r}_3 - \mathbf{r}_1$), a fixed scale factor (or distance parameter) g is introduced. Hence,

$$\mathbf{r}_2 = \mathbf{r}_1 + g(\mathbf{r}_3 - \mathbf{r}_1) \quad (6)$$

If the A–B bond distance $|\mathbf{r}_3 - \mathbf{r}_1|$ changes during a geometry optimization, the A–H bond distance $|\mathbf{r}_2 - \mathbf{r}_1|$ also changes. Derat et al. [53] have studied the ONIOM energy dependency as a function of the link atom bond distance ($r_2 - r_1$). They demonstrated that the ONIOM energies and optimized geometries do not depend on that scale factor, except for clearly “unreasonable” values of g . In the Gaussian 98 code [54], the reasonable bond length between the link atom and high-level layer atom (i.e. the scale factor g) is obtained by taking the ratio of the sum of the covalent radii of the set 2 (link) and set 1 atom to the sum of the covalent radii of the set 3 and the set 1 atom.

Because the positions of the link atoms are defined in terms of the atoms in the real system, the potential energy surface, and therefore geometry optimization, is well defined. The ONIOM gradient is obtained from

$$\frac{\partial E^{ONIOM}}{\partial \mathbf{R}} = \frac{\partial E_{\text{model system}}^{\text{high}}}{\partial \mathbf{R}} \cdot \mathbf{J} + \frac{\partial E_{\text{real system}}^{\text{low}}}{\partial \mathbf{R}} - \frac{\partial E_{\text{model system}}^{\text{low}}}{\partial \mathbf{R}} \cdot \mathbf{J} \quad (7)$$

where \mathbf{J} is the Jacobian, which is needed to convert the coordinate system for the model system to the coordinate system for the real system. The definition of the second derivatives of the ONIOM energy with respect to the nuclear coordinates, the Hessian matrix \mathbf{H}^{ONIOM} can be expressed in a similar fashion. The force constant matrix of the model system at low level and at high level have to be transformed by applying the Jacobian \mathbf{J} and its transposed \mathbf{J}^T .

$$\mathbf{H}^{ONIOM} = \mathbf{J}^T \frac{\partial^2 E_{\text{model system}}^{\text{high}}}{\partial \mathbf{R}^2} \cdot \mathbf{J} + \frac{\partial^2 E_{\text{real system}}^{\text{low}}}{\partial \mathbf{R}^2} - \mathbf{J}^T \frac{\partial^2 E_{\text{model system}}^{\text{low}}}{\partial \mathbf{R}^2} \cdot \mathbf{J} \quad (8)$$

The ONIOM method combines molecules of different size for energy calculations. As a consequence, one cannot define the wave function consistent with the ONIOM energy. However, the ONIOM density can be clearly defined as the sum and difference of the densities, as for the energy. For the two-layered ONIOM, the density is given as:

$$\rho^{ONIOM2} = \rho_{\text{model system}}^{\text{high}} + \rho_{\text{real system}}^{\text{low}} - \rho_{\text{model system}}^{\text{low}} \quad (9)$$

Thus, one-electron properties can be extrapolated as the energy and its derivatives.

The molecular properties related to an electric field \mathbf{F} can be easily found. The ONIOM2 dipole moment μ is given as:

$$\mu = \frac{\partial E^{ONIOM}}{\partial \mathbf{F}} = \frac{\partial E_{\text{model system}}^{\text{high}}}{\partial \mathbf{F}} + \frac{\partial E_{\text{real system}}^{\text{low}}}{\partial \mathbf{F}} - \frac{\partial E_{\text{model system}}^{\text{low}}}{\partial \mathbf{F}} \quad (10)$$

The polarizability tensor α is defined as:

$$\alpha = \frac{\partial^2 E^{ONIOM}}{\partial \mathbf{F}^2} = \frac{\partial^2 E_{\text{model system}}^{\text{high}}}{\partial \mathbf{F}^2} + \frac{\partial^2 E_{\text{real system}}^{\text{low}}}{\partial \mathbf{F}^2} - \frac{\partial^2 E_{\text{model system}}^{\text{low}}}{\partial \mathbf{F}^2} \quad (11)$$

and the third order hyperpolarizability tensor β becomes:

$$\beta = \frac{\partial^3 E^{ONIOM}}{\partial \mathbf{F}^3} = \frac{\partial^3 E_{\text{model system}}^{\text{high}}}{\partial \mathbf{F}^3} + \frac{\partial^3 E_{\text{real system}}^{\text{low}}}{\partial \mathbf{F}^3} - \frac{\partial^3 E_{\text{model system}}^{\text{low}}}{\partial \mathbf{F}^3} \quad (12)$$

The infrared intensities I_{IR} of molecular vibrations are derivatives with respect to the nuclear coordinates and hence, the Jacobian \mathbf{J} must be used again:

$$I_{IR} = \frac{\partial^2 E_{\text{model system}}^{\text{high}}}{\partial \mathbf{R} \partial \mathbf{F}} \cdot \mathbf{J} + \frac{\partial^2 E_{\text{real system}}^{\text{low}}}{\partial \mathbf{R} \partial \mathbf{F}} - \frac{\partial^2 E_{\text{model system}}^{\text{low}}}{\partial \mathbf{R} \partial \mathbf{F}} \cdot \mathbf{J} \quad (13)$$

Finally, the ONIOM Raman intensities I_{Raman} can be written as:

$$I_{Raman} = \frac{\partial^3 E_{\text{model system}}^{\text{high}}}{\partial \mathbf{R} \partial \mathbf{F}^2} \cdot \mathbf{J} + \frac{\partial^3 E_{\text{real system}}^{\text{low}}}{\partial \mathbf{R} \partial \mathbf{F}^2} - \frac{\partial^3 E_{\text{model system}}^{\text{low}}}{\partial \mathbf{R} \partial \mathbf{F}^2} \cdot \mathbf{J} \quad (14)$$

The corresponding equations for three- and n-layer ONIOM for all the derivative properties are derived and implemented in the same fashion.

5. RESULTS AND DISCUSSION

In the first part of the current section the performance of the ONIOM method was tested to reproduce the properties of the acid sites of zeolite ZSM-5. In the second part, the ONIOM method was used to model the structural, energetic and spectroscopic (IR and ^1H NMR) properties of the acid sites (type 1 and 2) of zeolite ZSM-5.

5.1 The test of the ONIOM method

Computational details

Three different crystallographic acid sites of zeolite ZSM-5 were chosen: Al3-O19-Si6, Al6-O18-Si9 and Al7-O17-Si4 (see Figure 2, numbering according to orthorhombic framework form [55]). The acid sites were modelled by the

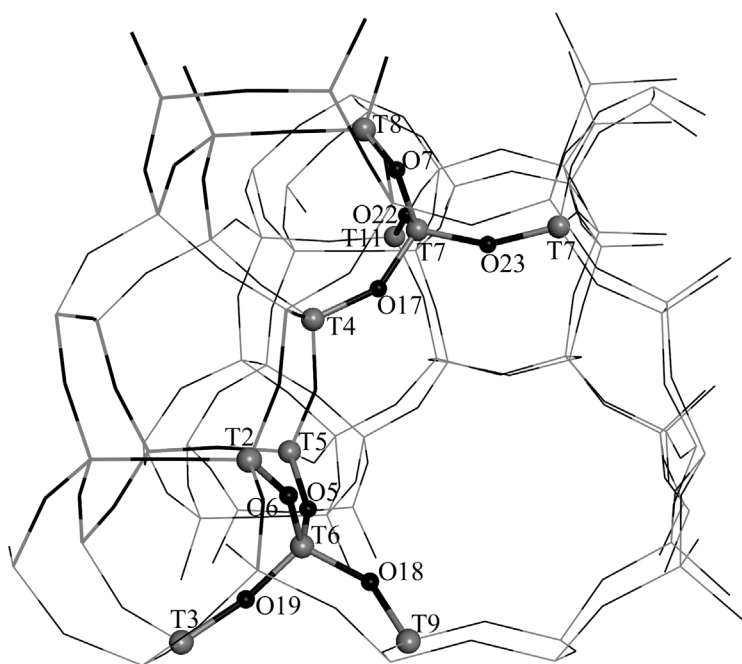


Figure 2. The locations of modelled acid sites viewed along sinusoidal channel.

two-layer ONIOM method using clusters consisting of 159–176 atoms or 46–51 T atoms (the real system). Chemically important inner part (the model system) was modelled using (i) two T atoms (1 Al and 1 Si atom) as a “2T model” (I shell in Figure 3) and (ii) 8 T atoms (1 Al and 7 Si atoms) as an “8T model” (II shell in Figure 3). Hydrogen atoms were used as link atoms and to saturate the dangling bonds of the whole cluster (the real system). In the other words, the model system included the first and the second shell of T atoms from the bridged hydroxyl group in the 2T and 8T model, respectively. Thus, the model systems were (with the hydrogens as link atoms) $\text{H}_3\text{Al-O(H)-SiH}_3$ and $(\text{H}_3\text{SiO})_3\text{-Al-O(H)-Si-(OSiH}_3)_3$. All studied clusters contained also a third shell of T atoms (Figure 3), which were connected with at least two other T atoms of the real system. This ensures rigidity of the zeolite framework around the acid site.

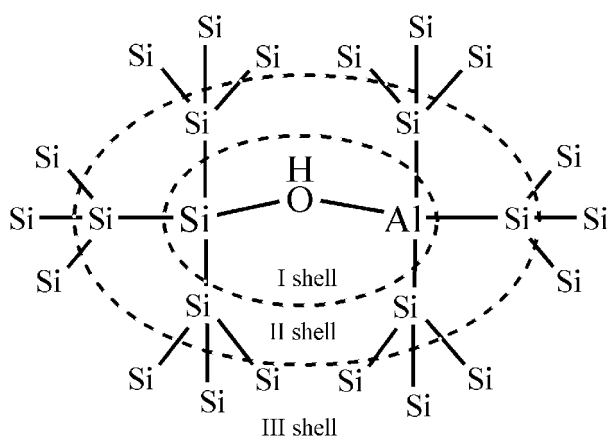


Figure 3. Illustration of layering of T atoms in used ONIOM schemes.

All calculations were performed using the Gaussian 98 [54] program package. The whole cluster (the real system) was calculated with MNDO method [56]. Model system part of the clusters was calculated with B3LYP/6-311+G** method and in a case of the 8T model, also at HF/6-31G* level of theory. No scaling was applied to obtained ONIOM(B3LYP/6-311+G**:
MNDO) frequencies for the calculations of thermodynamic parameters, while the ONIOM(HF/6-31G*:
MNDO) frequencies were scaled by factor 0.8929 [57]. The isotropic absolute (chemical) shielding constants were calculated for the model system part of the 8T cluster models with B3LYP/6-311+G** method on the ONIOM(B3LYP/6-311+G**:
MNDO) geometry using gauge including atomic orbitals (GIAO). For the ^1H NMR chemical shift calculations, methanol molecule was adopted as internal secondary standard for conversion

from the calculated isotropic absolute shielding constants σ to the chemical shift with respect to TMS, δ_{TMS} [58,59].

$$\delta_{\text{TMS}}(\text{Cluster}) = \delta_{\text{TMS}}(\text{CH}_3\text{OH}) + \sigma(\text{CH}_3\text{OH}) - \sigma(\text{Cluster}) \quad (15)$$

The calculated absolute shielding constant of hydroxyl proton, $\sigma(\text{CH}_3\text{OH})$, was 32.5 ppm and the used $\delta_{\text{TMS}}(\text{CH}_3\text{OH})$ is 0.02 ppm (experimental gas-phase value [60]).

Acidities and deprotonation enthalpies were calculated as the Gibbs free energy and enthalpy changes of reaction 16 taking into account zero-point energies, finite temperature (298 K) correction and the pressure-volume work term [61].



The interactions of CO with bridged hydroxyl group were characterized by Gibbs free energy and enthalpy changes of reaction 17.



For an additional comparison of the strength of the different acid sites the energies of reactions 16 (deprotonation energies) and 17 (adsorption energies) were calculated from the total energy changes of the model system, calculated at HF/6-31G* and B3LYP/6-311+G** levels, respectively.

Results of the test calculations

Calculated geometry parameters of the bridged hydroxyl groups in three different crystallographic position are presented in Table 2. From the comparison of the bond lengths calculated on the 8T cluster models using the ONIOM(B3LYP/6-311+G**):MNDO) and the ONIOM(HF/6-31G*):MNDO) methods, one can see that as a rule the ONIOM(HF/6-31G*):MNDO) bond lengths are the shortest. It is known that HF method predicts too short bond lengths [63] — in the case of O–H bonds the maximum deviation in bond lengths calculated with the ONIOM(HF/6-31G*):MNDO) method from bond lengths calculated with the ONIOM(B3LYP/6-311+G**):MNDO) method is 0.02 Å. The Al-O and Si-O bonds of bridged hydroxyl groups are calculated to be too long in 2T clusters compared to the 8T cluster model calculated with the same ONIOM(B3LYP/6-311+G**):MNDO) method. These bonds are associated with atoms that are on the border of model and real systems, thus the link atoms that are present during the model system calculations have strong effect on neighboring bonds.

Table 2. Calculated geometry parameters of the bridged hydroxyl groups in a three different crystallographic position (bond lengths in Å, bond angles in degrees).

	Al3-O19-Si6			Al6-O18-Si9			Al7-O17-Si4		
	ZH	Z ⁻	ZH...CO	ZH	Z ⁻	ZH...CO	ZH	Z ⁻	ZH...CO
8T	ONIOM(HF/6-31G*:MND0)								
O-H	0.9552		0.9580	0.9541		0.9582	0.9532		0.9564
Al-O	1.9828	1.7708	1.9775	1.9265	1.7590	1.9212	1.9479	1.7650	1.9413
Si-O	1.7092	1.5748	1.7074	1.6911	1.5711	1.6876	1.6852	1.5694	1.6830
Al-O-H	102.47		104.22	108.32		110.27	106.97		109.63
Si-O-H	112.27		111.26	116.44		115.46	117.75		116.69
Al-O-Si	144.94	166.31	144.43	132.53	140.70	132.56	133.30	145.86	133.00
Al...H ^a	2.3795		2.3998	2.4035		2.4258	2.4057		2.4353
O-H...CO			2.3196			2.2263			2.3197
2T	ONIOM(B3LYP/6-311+G**):MND0)								
O-H	0.9653		0.9712	0.9638		0.9715	0.9638		0.9699
Al-O	2.2367	1.8149	2.2098	2.0647	1.8026	2.0559	2.1452	1.8038	2.1286
Si-O	1.7343	1.6295	1.7306	1.7225	1.6241	1.7188	1.7142	1.6181	1.7118
Al-O-H	101.76		102.38	110.65		111.96	108.86		111.12
Si-O-H	112.44		112.68	116.25		115.77	116.55		115.53
Al-O-Si	145.74	166.38	144.93	132.05	143.1	131.77	134.09	155.95	133.23
Al...H ^a	2.6105		2.5974	2.5681		2.5816	2.6206		2.6380
O-H...CO			2.2412			2.1665			2.2325
8T	ONIOM(B3LYP/6-311+G**):MND0)								
O-H	0.9695		0.9780	0.9670		0.9785	0.9671		0.9748
Al-O	1.9864	1.7811	1.9780	1.9265	1.7697	1.9188	1.9535	1.7758	1.9438
Si-O	1.7265	1.5920	1.7227	1.7056	1.5867	1.7001	1.6984	1.5845	1.6955
Al-O-H	101.13		103.579	108.34		110.74	105.88		110.875
Si-O-H	112.59		111.314	116.93		115.66	118.47		115.954
Al-O-Si	145.87	166.79	145.072	132.85	141.78	132.77	134.29	148.16	132.961
Al...H ^a	2.3726		2.4035	2.4122		2.4431	2.4053		2.4656
O-H...CO			2.1168			2.0266			2.1253

^a Exp. 2.48 ± 0.04 [63] and 2.43 ± 0.03 [64].

H-Al distance can be determined from NMR spectroscopic measurements [12]. Calculated H-Al distances of the 8T models are in good agreement with the experimental values [63,64] for zeolite ZSM-5, only the H-Al distance in Al3-O19(H)-Si6 site is somewhat short. H-Al distances are overestimated in case of 2T model. The bond angles calculated with different ONIOM combinations are in surprisingly good accordance with each other. Average deviations between Al-O(H)-Si bond angles do not exceed 0.75° . The biggest differences can be found between Al-O-Si bond angles in the 2T and 8T anionic clusters indicating that the bonds near the border of the model system are treated less satisfactory in case of too small model system. Differences in calculated geometry parameters of bridged hydroxyl groups in different crystallographic posi-

tions show that ONIOM method can differentiate between acid sites in different crystallographic positions.

Calculated deprotonation energies, deprotonation enthalpies and acidities for studied cluster models are presented in Table 3. The acidities of 8T model calculated with the ONIOM(B3LYP/6-311+G**):MNDO) method are the highest, ONIOM(HF/6-31G*:MNDO) acidities are 3.4-4.6 kcal/mol smaller. The relative acidities of different acid sites (acidity differences relative to acidity of a Al7-O17-Si4 site) calculated on the 8T cluster with different ONIOM models are within 0.6 kcal/mol. The deprotonation enthalpies calculated on 2T cluster models are about 13.3 kcal/mol higher (acidities are lower) compared to the 8T model (using the ONIOM(B3LYP/6-311+G**):MNDO) method) and the differences in relative acidities of different acid sites are bigger (up to 2.1 kcal/mol). This indicates that inclusion of a next shell of T atoms (silicon atoms) around bridged hydroxyl group into the model system lowers deprotonation energy by about 13 kcal/mol (difference between 2T and 8T model system deprotonation energies calculated at the same level of theory). Adding additional shells of T atoms (calculated at the MNDO level) around model system, however, raises the deprotonation energy (differences between deprotonation energies of the model and the real system). To investigate this inconsistency we have made single point calculations, where a shell of T atoms around an the 8T model system is treated at HF/3-21G* level of theory on an ONIOM(HF/6-31G*:MNDO) geometry. The calculations on the same systems using DFT or ab initio methods instead of MNDO method show that in case of MNDO method the deprotonation energies are systematically overestimated by about 9 kcal/mol. Systematic errors in real system calculations have, thus, systematic effect on ONIOM extrapolated energy.

Table 3. Calculated deprotonation energies (ΔE), deprotonation enthalpies (ΔH_{acid}) and acidities (ΔG_{acid}) at ONIOM geometry. All values in kcal/mol.

		ΔE	ΔE	ΔH_{acid}	ΔG_{acid}
		Model system	Real system		
		HF/6-31G*	ONIOM(HF/6-31G*:MNDO)		
8T	Al3-O19H-Si6	299.7	317.4	311.5	303.3
	Al6-O18H-Si9	302.4	320.9	315.0	306.9
	Al7-O17H-Si4	303.0	324.4	318.5	311.1
		Model system	Real system		
		B3LYP/6-311+G**	ONIOM(B3LYP/6-311+G**):MNDO)		
2T	Al3-O19H-Si6	309.8	327.4	321.2	313.8
	Al6-O18H-Si9	313.1	329.0	322.7	314.6
	Al7-O17H-Si4	312.3	333.6	327.3	319.4
8T	Al3-O19H-Si6	296.2	313.3	307.0	298.8
	Al6-O18H-Si9	298.8	316.6	310.4	302.1
	Al7-O17H-Si4	299.9	320.5	314.3	306.5

The comparison of the deprotonation energies of the model and the real system (ONIOM energy) reveals that the main contribution to the deprotonation energies comes from the model system (~95%), thus, to the first approximation the model system is like a cluster embedded in the real system framework which holds the model system in the crystallographic conformation. In this approach the deprotonation energies calculated with the same high-level method on the same size systems are being compared, excluding the systematic erroneous contribution to the deprotonation energy by the lower level calculations. As can be seen from the real systems deprotonation energy and deprotonation enthalpy differences, the zero-point energies and thermal corrections for used clusters are rather constant — lowering the deprotonation energy by about 6.3 kcal/mol in case of the ONIOM(B3LYP/6-311+G**):MND) method. Thus, taking into account the zero-point energies and the thermal corrections from the frequency calculations, the deprotonation enthalpies of the 8T model systems (at 298K) calculated with B3LYP/6-311+G** method are 289.9, 292.5 and 293.7 kcal/mol for Al3-O19(H)-Si6, Al6-O18(H)-Si9 and Al7-O17(H)-Si4 sites, respectively, and being in good accordance with experimental [65] and previous theoretical [24,26,31] studies of zeolite ZSM-5.

Table 4 lists calculated and experimental stretching vibrational frequencies of: (i) the bridged hydroxyl groups, (ii) the hydroxyl groups in the complex with CO, and (iii) vibrational frequency shifts of the hydroxyl groups upon adsorption of CO. Experimental frequencies of bridged hydroxyl groups of the zeolite ZSM-5 are in the range of 3590–3627 cm^{-1} [4,11,66–68] and $\sim 3250 \text{ cm}^{-1}$ [3,7] depending on temperature and composition. Upon adsorption of carbon monoxide, the stretching frequencies of bridged hydroxyl groups (at 3590–3627 cm^{-1}) undergo a red shift by about 305–340 cm^{-1} [69,70]. Scaled harmonic frequencies of bridged hydroxyl groups obtained with the ONIOM(HF/6-31G*:MND) method are in the experimentally determined range but the frequency shifts upon interaction with CO are too small (46–69 cm^{-1} against 305–340 cm^{-1} in experiment). Inclusion of electron correlation increases the red shift, in the case of the 8T cluster model the shifts in stretching frequencies of bridged hydroxyl groups calculated with the ONIOM(B3LYP/6-311+G**):MND) method are in the range of 170–253 cm^{-1} . Somewhat smaller frequency shifts calculated on the 2T cluster model indicates again that 2T model system is too small to take the short-range interactions into account correctly.

Table 4. Calculated and experimental stretching vibrational frequencies (ω) of the bridged hydroxyl groups, the hydroxyl groups in the complex with CO, and vibrational frequency shifts ($\Delta\omega$) of the hydroxyl groups upon adsorption of CO. All values in cm^{-1} .

		Al3-O19-Si6	Al6-O18-Si9	Al7-O17-Si4	Exp.
ONIOM(HF/6-31G*:MNDO)					
	ω OH	3595	3617	3622	3590 ... 3627 ^b
8T ^a	ω OH...CO	3549	3548	3574	
	$\Delta\omega$	-46	-69	-49	-305 ... -340 ^c
ONIOM(B3LYP/6-311+G**):MNDO)					
	ω OH	3826	3853	3851	3590 ... 3627 ^b
2T	ω OH...CO	3705	3691	3725	
	$\Delta\omega$	-121	-163	-126	-305 ... -340 ^c
ONIOM(B3LYP/6-311+G**):MNDO)					
	ω OH	3765	3812	3802	3590 ... 3627 ^b
8T	ω OH...CO	3585	3559	3632	
	$\Delta\omega$ (OH)	-180	-253	-170	-305 ... -340 ^c

^a scaled with 0.8929.

^bRefs. [4,11,66–68].

^cRefs. [69,70].

Previous quantum chemical calculations [70,71,72] have shown that the anharmonicity must be taken into consideration in reproducing the vibrational frequencies of the O–H bonds in zeolites. The IR measurements [70,73,74] and quantum chemical calculations [70,75–77] have shown that anharmonicity parameters $\omega_e x_e$ of the bridged hydroxyl groups are in range of 76–102 cm^{-1} , depending on used method and cluster. The anharmonicity parameter for hydroxyl groups is reported to be rather constant, and it is assumed that the anharmonicity constant is independent both from the type as well the environment of the hydroxyl group [73,76]. An increase in anharmonicity in OH stretch motion is observed when hydroxyl group is in stronger interactions with adsorbed molecules [70,74]. Senchenya et al. [70] estimated based on experimental measurements the anharmonicity parameter for the zeolite Mordenite to be 95 cm^{-1} in case of the bridged hydroxyl group and 136 cm^{-1} in case of the hydroxyl group in interaction with CO. As there is no information about anharmonicity parameter for zeolites ZSM-5 bridged hydroxyl groups or for bridged hydroxyl groups in interaction with CO, we can only approximately correct our calculated harmonic vibrational frequencies with anharmonicity parameters determined by Senchenya for better comparison with experimentally observed anharmonic frequencies. For the vibrational frequencies of the bridged hydroxyl groups obtained with the ONIOM(B3LYP/6-311+G**):MNDO) method we get 3575, 3622 and 3612 cm^{-1} for the Al3-O19H-Si6, Al6-O18H-Si9 and Al7-O17H-Si4

sites, respectively, and for the shifts in stretching vibrational frequencies upon interaction of carbon monoxide we get -262 , -335 and -252 cm^{-1} for the Al3-O19H-Si6, Al6-O18H-Si9 and Al7-O17H-Si4 sites respectively. With the anharmonicity parameter corrected stretching vibrational frequencies of bridged hydroxyl groups at Al6-O18H-Si9 and Al7-O17H-Si4 site are in good agreement with experimental measurements.

The collection of experimental ^1H NMR chemical shifts for bridged hydroxyl groups is presented in Table 1. The changes in ^1H NMR chemical shifts of hydroxyl groups upon adsorption of carbon monoxide is 1.8 – 2.0 ppm [7,78]. Calculated results (Table 5) show again the best agreement with experimental data in case of the Al6-O18H-Si9 site. In case of the Al7-O17H-Si4 site the ^1H NMR chemical shift is close to experimental value but the shift in ^1H NMR chemical shift of hydroxyl groups upon adsorption of CO is somewhat underestimated compared to experimental findings.

Table 5. The experimental and calculated ^1H NMR chemical shifts (δ) of the bridged hydroxyl groups, the bridged hydroxyl groups in interaction with CO and shifts in ^1H NMR chemical shifts ($\Delta\delta$) of hydroxyl groups upon adsorption of CO. All values in ppm.

		ONIOM(B3LYP/6-311+G**):MNDO			Exp ^a .
		Al3-O19H-Si6	Al6-O18H-Si9	Al7-O17H-Si4	
	$\delta(\text{OH})$	3.7	4.3	4.0	4.2 ± 0.1
8T	$\delta(\text{OH}\cdots\text{CO})$	4.8	6.1	5.2	6.2
	$\Delta\delta$	1.1	1.8	1.2	1.8 – 2.0

^a Ref. [7,22,78].

Conclusions

The results of calculations show that the ONIOM method (using HF/6-31G* or B3LYP/6-311+G** method for describing the model system and MNDO method for describing the real system) can differentiate between the crystallographically different acid sites. For reproducing the properties of the acid sites of zeolite ZSM-5 accurately, the size of the model system should extend at least to eight T atoms. It is also important that computational methods used take into account electron correlation and the anharmonicity of stretch motion of the bridged hydroxyl groups.

5.2 Calculation of the properties of acid sites in zeolite ZSM-5

Computational details

Two different aluminium atom locations (at the T6 and the T7 site [55]) were chosen, and all four acid sites that form when protons are attached to one of the oxygen atoms bonded directly to the aluminium atom were studied (for details see Tables 6 and 7; Figure 2). Those locations (for Al atom) have been associated with the most probable acid sites in zeolite ZSM-5 by previous theoretical studies [32,79]. The acid sites were modelled by the three-layer ONIOM method using clusters (the real system) consisting of 108 T atoms (1 Al and 107 Si atoms; see Figure 4). The high-level (B3LYP/6-311+G**) model system part includes two complete coordination shells of T-atoms around central hydroxyl group (8T model, $(\text{H}_3\text{SiO})_3\text{-Si(OH)Al-(OSiH}_3)_3$). The middle system, treated at medium level of theory (HF/3-21G*), enfolds another complete shell of T-atoms around high-level model system. Hydrogen atoms are used as link atoms and to saturate the dangling bonds of the whole cluster (real system). The distances corresponding to the bonds between link atoms (hydrogens) and silicon atoms in the model system are defined to be proportional to Si-O distances in the real system (standard proportionality factor $g = r(\text{Si-H})/r(\text{Si-O}) = 0.862$ is used in Gaussian98 [54]). The clusters, modelling hydroxyl groups involved in hydrogen bonding, are calculated additionally with an alternative partitioning scheme, where the model system is extended at the expense of middle system to cover complete rings involved in H-bond formation (Figure 4C).

All calculations were performed using the standard implementation of the ONIOM method in Gaussian 98 [54] program package. Full geometry optimisations were carried out with the ONIOM(B3LYP/6-311+G**: $\text{HF/3-21G*}:\text{MNDO}$) method for all clusters studied. To locate bridged hydroxyl groups of the second type, we used different starting geometries in the case of each acid site.

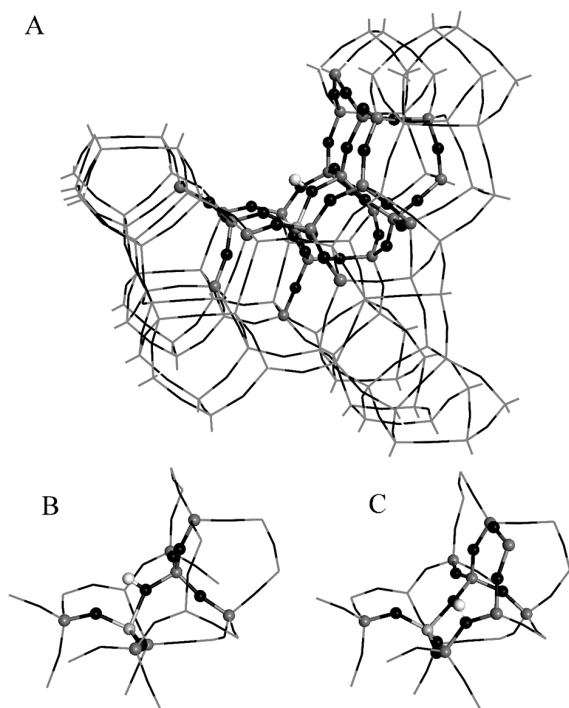


Figure 4. Illustration of the used partitioning schemes in case of Al₇-O₇(H)-Si₈ acid site. The used cluster (real system) with high and medium level parts is shown in ball and stick style (A). The first type of bridged hydroxyl group calculated with the 8T size model system (ball and stick style) surrounded by middle system is shown in line style (B). The second type of bridged hydroxyl group calculated with extended size model system (ball and stick style) surrounded by middle system is shown in line style (C).

Like shown previously, using the MNDO method in the calculation of the energies of low-level real system results in energies that have a systematic erroneous contribution to the ONIOM deprotonation energies of zeolites. To avoid this inaccuracy, we chose to omit the MNDO contribution from ONIOM3 energies and to use only high- and medium-level energies from the ONIOM3 calculations. Therefore, used energetic properties are extrapolated only from energies calculated at high- and medium-level (ONIOM2(B3LYP/6-311+G**:*HF/3-21G**)) and are named ONIOM2 energies. Deprotonation energies were calculated as ONIOM2 energy changes of reaction 16 (at 0 K).

Experimental [70,73] and computational studies [72,76,80] have shown that the O-H stretch mode is essentially a pure mode; that is, it is uncoupled from all other vibrations of the zeolite framework, and therefore the bridging hydroxyls can be treated as isolated diatomic fragments, O-H. Meijer et al. have recently shown [81] that in the case of strong hydrogen bonding with adsorbed base the

stretch-bend interactions might be considerable. Still, we have, in the current work, assumed that for the studied systems with the relatively weak hydrogen bonding the bridging hydroxyl can be treated as isolated diatomic fragment. Because the standard frequency calculations were prohibitively expensive for us and we are mainly interested in stretching vibrational frequencies of bridged hydroxyl groups, the anharmonic stretching vibrational frequencies of bridged hydroxyl groups were estimated as follows. A series of single point calculations was performed at various fixed O-H bond length whereas other atoms were kept fixed in their equilibrium positions. The O-H bond lengths were varied by ± 0.25 Å from the equilibrium bond length in steps of 0.05 Å. The obtained potential energy surface was fit to Morse function from which the anharmonicity constant and vibrational frequencies were determined [71,82]. The standard deviation of the calculated points from Morse curve was less than 0.3 millihartrees. This approach has shown good results in previous studies of modelling OH vibrations in zeolites [71,80,82].

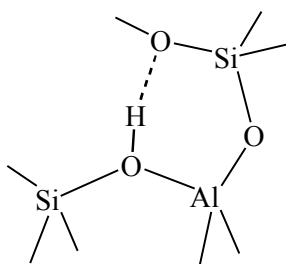
^1H NMR chemical shifts have been evaluated from the isotropic absolute (chemical) shielding constants σ obtained according to formula 18 using gauge including atomic orbitals (GIAO).

$$\sigma^{\text{ONIOM2(B3LYP/6-311+G**;HF/3-21G*)}} = \sigma_{\text{model system}}^{\text{B3LYP/6-311+G**}} + \sigma_{\text{middle system}}^{\text{HF/3-21G*}} - \sigma_{\text{model system}}^{\text{HF/3-21G*}} \quad (18)$$

For a reference, tetramethylsilane, computed at the B3LYP/6-311+G** level of theory ($\sigma_{\text{TMS}} = 31.98$ ppm), was used.

Results and discussion

Both types of bridged hydroxyl groups (type 1 and 2) are represented among the studied acid sites (shown in Figure 4). In the case of the second type of Brønsted acid site, the hydrogen of the bridged hydroxyl group forms a hydrogen bond with the next nearest oxygen to the aluminium atom (Scheme 1).



Scheme 1. Schematic representation of the hydrogen bond formation in case of the second type of Brønsted acid site.

Tables 6 and 7 present a selection of calculated geometry parameters of the bridged hydroxyl groups in studied crystallographic positions. The length of calculated hydrogen bonds are between 1.7622–1.8810 Å, where the hydrogen bonds in five-membered rings (Al6-O6(H)-Si2 and Al6-O19(H)-Si3 sites) are somewhat longer than those in six-membered rings (Al7-O7(H)-Si8 and Al7-O22(H)-Si11 sites). The O-H bond lengths of hydroxyl groups, which are influenced by a hydrogen bond, are about 0.02 Å longer than the O-H bond lengths in free hydroxyl groups.

Table 6. Calculated geometry parameters of the bridged hydroxyl groups formed around aluminium at T6 site (bond length in Å, bond angles in degrees)

	Al6-O6-Si2		Al6-O19-Si3		Al6-O5-Si5	Al6-O18-Si9
	free	H-bonded	H-bonded	H-bonded	free	free
O-H	0.9703	0.9955	0.9881	0.9882	0.9741	0.9721
OH...O	2.3251 ^a	1.7828 ^b	1.8368 ^c	1.8810 ^d	2.1516 ^a	2.2286 ^e
Al-O(H)	1.9766	1.9577	1.9511	1.9704	1.9196	1.9137
Si-O(H)	1.7117	1.7061	1.7082	1.7111	1.6935	1.6918
Al-O-H	101.06	103.96	107.64	104.52	99.72	102.28
Si-O-H	115.77	117.00	109.70	116.87	115.20	116.88
O-Al-O(H)	90.42	95.46	95.68	95.96	87.41	88.84
Al-O(H)-Si	142.66	136.36	141.24	137.86	144.73	140.83

distance to: ^aO18; ^bO4; ^cO11; ^dO8; ^eO5

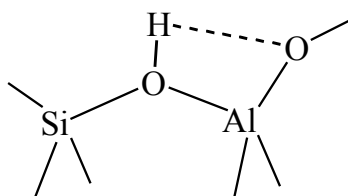
Table 7. Calculated geometry parameters of the bridged hydroxyl groups formed around aluminium at T7 site (bond length in Å, bond angles in degrees)

	Al7-O17-Si4	Al7-O23-Si7	Al7-O7-Si8		Al7-O22-Si11
	free	free	free	H-bonded	H-bonded
O-H	0.9710	0.9695	0.9714	0.9966	0.9977
OH...O	2.2833 ^a	2.4398 ^b	2.2217 ^c	1.7747 ^d	1.7622 ^c
Al-O(H)	1.9578	1.9266	1.9612	1.9484	1.9211
Si-O(H)	1.6987	1.7060	1.6952	1.6903	1.6902
Al-O-H	102.32	106.27	100.26	104.72	106.06
Si-O-H	114.64	115.06	117.51	119.15	119.88
O-Al-O(H)	89.24	93.40	88.02	95.06	96.23
Al-O(H)-Si	138.55	138.53	142.00	134.65	132.66

distance to: ^aO23; ^bO17; ^cO22; ^dO7

In protonated (neutral) zeolites, the comparison of bond lengths and bond angles associated with aluminium atom shows that the Al-O(H) bond lengths are about 0.2 Å longer than Al-O(Si) bonds and O-Al-O(H) bond angles are decreased by 8.4° on average, compared to those for the anionic form, whereas O-Al-O bond angles are increased by 6.9°, resulting in average O-Al-O bond angle of 116.5°. This distortion of the local environment around Al toward a slightly trigonal coordination has also been reported previously by other computational studies [31,42,83,84], and it was used to explain the line broadening and the large quadrupole coupling constant in the ²⁷Al NMR spectra of dehydrated H-zeolites [84,85].

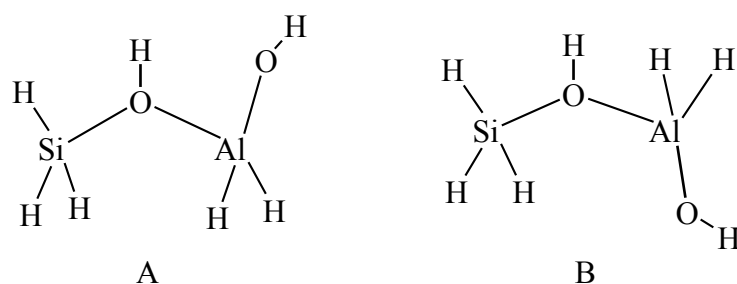
The distances from hydrogen (in the first type of bridged hydroxyl group, see Scheme 2) to the nearest oxygen (bonded to aluminium) are quite small, ranging from 2.1516 Å to 2.4398 Å. The comparison of O-Al-O(H) angles at different Al centres shows that the angles involving oxygens nearest to the hydroxyl groups' hydrogens are also about 17° smaller than the rest of O-Al-O(H) angles. In our opinion, those contracted O-Al-O(H) angles (average bond angle is 89.6°) and small Al-O-H angles (an average bond angle is 102.0°) are most likely caused by the electrostatic interaction between hydrogen in the first type of bridged hydroxyl group and the nearby framework oxygen (Scheme 2).



Scheme 2. Schematic representation of an electrostatic interaction between hydrogen atom in the first type of bridged hydroxyl group and the nearest oxygen of zeolites framework.

For the quantitative estimation of the strength of that electrostatic interaction, additional calculations were performed with small clusters presented in Scheme 3.

The energy difference between fully optimised (at B3LYP/6-311+G** level of theory) conformers A and B (from Scheme 3) is 1.3 kcal/mol; thus, the energy of that interaction is small but definitely not negligible.



Scheme 3. Schematic representation of used clusters for quantitative estimation of the electrostatic interaction between hydrogen in bridged hydroxyl group and nearby oxygen.

The geometries, calculated on the clusters with extended model system, are very similar to those that are calculated with the 8T size model system (see Table 8). The effect of the inclusion of the electron correlation on all atoms involved in hydrogen bonding can be witnessed by somewhat decreased O-H bond lengths and up to 0.3 Å increased hydrogen bond lengths. As a result, the second type of hydroxyl group in Al6-O19-Si3 site (with hydrogen bond to O11) changes to the first type of hydroxyl group (closest oxygen to the hydroxyl hydrogen is O5).

Table 8. Geometry parameters of the second type of bridged hydroxyl groups calculated on clusters with extended model system (bond length in Å, bond angles in degrees)

	Al6-O6-Si2	Al6-O19-Si3	Al7-O7-Si8	Al7-O22-Si11	
O-H	0.9826	0.9760	0.9771	0.9831	0.9843
OH...O	1.9869 ^a	2.1590 ^b	2.1810 ^c	1.9981 ^d	1.9565 ^e
Al-O(H)	1.9641	1.9692	1.9765	1.9560	1.9279
Si-O(H)	1.7109	1.7083	1.7161	1.6958	1.6960
Al-O-H	104.41	97.15	104.60	105.95	107.67
Si-O-H	114.06	113.44	113.77	116.16	116.69
O-Al-O(H)	96.22	87.71	96.02	95.50	97.15
Al-O(H)-Si	139.35	148.12	141.46	136.42	134.22

distance to: ^aO4; ^bO5 (distance to O11 is 2.5043Å); ^cO8; ^dO7; ^eO22

Calculated deprotonation energies of the studied hydroxyl groups (Tables 9 and 10) are in good accordance with experimental estimations [65] and previous theoretical studies [24,26,31] of zeolite ZSM-5. From the comparison of the deprotonation energies of hydroxyl groups in different crystallographic positions, estimations of the relative stabilities of different acid sites can be made. The

larger the deprotonation energy, the harder it is to detach a proton from the zeolite's framework, and thus, the proton for a given T-site is expected to locate on the oxygen with the greatest deprotonation energy. In both studied aluminium sites, the calculated deprotonation energies of the second type of bridged hydroxyl groups are the highest as upon deprotonation additional energy is needed for breaking the hydrogen bonds. This is also evidenced by low-temperature ^1H MAS NMR investigations of the interactions between surface hydroxyl groups and CO molecules [12], where at low coverage only the signal from the first type of bridged hydroxyl groups is affected by adsorbed CO in contrast to the signal from the second type of bridged hydroxyl groups that remain unperturbed.

The strength of hydrogen bonds can be estimated from the comparison of the deprotonation energies of free and hydrogen bonded bridged hydroxyl groups in the same crystallographic position. Obtained hydrogen bond energies are 4.3 and 5.1 kcal/mol for Al6-O6-Si2 and Al7-O7-Si8 sites, respectively.

The deprotonation energies calculated on the clusters with extended model system are up to 3.1 kcal/mol lower than deprotonation energies calculated on the clusters with the 8T size model system. The weakening of hydrogen bonds (hydrogen bond energies are 1.9 and 2.0 kcal/mol for Al6-O6-Si2 and Al7-O7-Si8 sites respectively) after inclusion of the electron correlation in all atoms involved in hydrogen bonding is consistent with the increase of hydrogen bond length in analogous comparison.

Table 9. Calculated deprotonation energies (DPE, in kcal/mol), ^1H NMR chemical shifts (δ , in ppm) and stretching vibrational frequencies (ω , in cm^{-1}) of studied bridged hydroxyl groups formed around aluminium at T6 site

	Al6-O6-Si2		Al6-O19-Si3		Al6-O5-Si5	Al6-O18-Si9
	free	H-bonded	H-bonded ^a	H-bonded ^b	free	free
DPE	290.0	294.3	289.6	292.8	291.6	292.4
DPE ^c	289.7	291.9	289.6	289.8		
$\delta(\text{OH})$	3.9	7.3	6.7	6.4	5.2	4.9
$\delta(\text{OH})^c$	3.8	6.3	5.1	5.2		
$\omega(\text{OH})$	3615	2897	3124	3104	3550	3588
$\omega(\text{OH})^c$	3626	3291	3512	3432		

^a hydrogen bond with O11, in case of clusters calculated with extended model system the second type of bridged hydroxyl group is changed to the first type of bridged hydroxyl group, where the closest oxygen to the hydroxyl hydrogen is O5; ^b hydrogen bond to O8; ^c calculated using clusters with extended model system

Table 10. Calculated deprotonation energies (DPE, in kcal/mol), ^1H NMR chemical shifts (δ , in ppm) and stretching vibrational frequencies (ω , in cm^{-1}) of studied bridged hydroxyl groups formed around aluminium at T7 site

	Al7-O17-Si4	Al7-O23-Si7	Al7-O7-Si8		Al7-O22-Si11
	free	free	free	H-bonded	H-bonded
DPE	290.9	290.8	290.5	295.6	296.9
DPE ^a			290.5	292.5	294.5
$\delta(\text{OH})$	4.2	4.3	4.5	7.7	8.0
$\delta(\text{OH})^a$			4.4	6.5	7.0
$\omega(\text{OH})$	3608	3639	3587	2847	2829
$\omega(\text{OH})^a$			3592	3273	3248

^a calculated using clusters with extended model system

Our estimated vibrational frequencies of hydrogen bonded hydroxyl groups calculated on clusters with the 8T size model system are ranging from 2829 to 3124 cm^{-1} , frequencies calculated on clusters with extended model system are about 400 cm^{-1} higher and, as a result, are in better agreement with experimental measurements. The calculated stretching frequency (3432 cm^{-1}) of the hydroxyl group in Al6-O19-Si3 site with hydrogen bond to O8 is approximately 160 cm^{-1} higher compared to other three OH groups involved in hydrogen bonding (the frequencies ranging from 3248 to 3291 cm^{-1}). This can be explained by the comparative weakness of that hydrogen-bond which is also evidenced by the longest hydrogen bond length and small deprotonation energy.

In general, calculated vibrational frequencies of the first type of bridged hydroxyl groups are well in the range of experimental findings (Tables 9 and 10). Datka et al. [4] have shown that the IR band (at $\sim 3610 \text{ cm}^{-1}$) of the first type of bridged hydroxyl groups can be split into several submaxima that are located between 3590 and 3627 cm^{-1} . Our estimated vibrational frequencies are in good agreement with those experimental findings; that is, different IR absorption submaxima are well reproduced by our ONIOM calculations. The distribution of calculated frequencies is somewhat wider than experimentally determined, probably because not all acid sites calculated here are sufficiently populated (discussed in detail in the next sections). For example, the Al6-O19-Si3 site, where the calculated vibrational frequency differs from experimental ones by 78 cm^{-1} , is energetically the most unfavourable for proton attachment (by 2.8 kcal/mol compared to the site with highest proton affinity in case of formation of the first type bridged hydroxyl groups) and thus is hardly populated. On the other hand, the deprotonation energies of the first type of bridged hydroxyl groups around Al in T7 site differ only by 0.4 kcal/mol and the corresponding vibrational frequencies are well in the experimental range.

The comparison of experimentally measured (Table 1) and calculated ^1H NMR chemical shifts of both types of bridged hydroxyl groups shows (Tables 9

and 10) that ^1H NMR chemical shifts of the both types of bridged hydroxyl groups calculated with the ONIOM method are in good accordance with experimental measurements. Again, like in the case of IR spectra, the distribution of calculated ^1H NMR chemical shifts of the first type of bridged hydroxyl groups is somewhat wider (the distribution range is 1.3 ppm, from 3.9 to 5.2 ppm) than experimentally determined, probably because all sites do not get populated at moderate temperatures as discussed below.

On the basis of our calculation, some refinements can be made to the Freude's model describing the relations between the first and the second type of bridged hydroxyl groups [9]. At lower temperatures in some crystallographic positions, the bridging hydroxyl groups can form hydrogen bonds with nearby oxygen atoms, as described in Scheme 1. With increasing temperature, the hydrogen bonds start to break, as evidenced by the decrease of the corresponding IR and ^1H NMR spectral lines [3,8]. At the same time, the increase of the band of the first type of bridged hydroxyl groups indicates that the second type of bridged hydroxyl group is transformed into the first type of bridged hydroxyl group. In our calculation, this is revealed in crystallographic positions Al6-O6-Si2 and Al7-O7-Si8, where both type of bridged hydroxyl groups can be formed.

With a further increase in temperature, the protons gain sufficient energy to overcome the activation barrier to move between neighbouring oxygen atoms in AlO_4 unit [22,86,87]. As a consequence, the bridged hydroxyl groups with slightly different spectroscopic properties (with different vibrational frequencies or ^1H NMR chemical shifts) can be formed, and this results in the increase of the width of spectral bands of the first type of bridged hydroxyl groups. The shift of the IR band maximum toward the lower frequencies indicates that at higher temperatures the bridged hydroxyl groups with lower vibrational frequencies dominate in the overall set of OH groups.

As mentioned previously, the probability of finding a proton attached to a certain oxygen in AlO_4 tetrahedron depends on deprotonation energies of the corresponding protonation centres. Our calculations show that in the case of acid sites around the aluminium located at crystallographic position T6 the proton abstraction energy is highest from Al6-O18-Si9 site. The OH group formed in Al6-O18-Si9 site has also lower vibrational frequency (3588 cm^{-1}) than the free OH group formed after hydrogen bond breaking in Al6-O6-Si2 site (3615 cm^{-1}). The calculated difference in vibrational frequencies (27 cm^{-1}) is in good agreement with the experimentally observed redshift (20 cm^{-1}) in vibrational frequencies ongoing from 300 K to 770 K [3]. This indicates that at lower temperatures (after breaking the hydrogen bond) the occupancies of protons at various oxygen sites is kinetically controlled and thermodynamic equilibrium is reached at high temperatures. Thus, in wide temperature range, when, at different temperatures, acid sites with different acid strengths dominate among all acidic centres present, the experimentally observable mean acidity of zeolite ZSM-5 depends on temperature.

Conclusions

The Brønsted acid sites in eight different crystallographic position of the zeolite ZSM-5 were modelled by the ONIOM3(B3LYP/6-311+G**:^{HF}/3-21G*:^{MNDO}) method. Both types of bridged hydroxyl groups (type 1 and 2) were represented among the studied acid sites.

Our calculations show that in the case of the second type of Brønsted acid site, the hydrogen of the bridged hydroxyl group forms a hydrogen bond with one of the lattice oxygen atoms. In the case of the first type of bridged hydroxyl groups, the distortion of the local environment around Al indicates that hydrogen atoms in the first type of bridged hydroxyl groups are also influenced by an electrostatic interaction (primarily) with nearby oxygen atoms.

The results of calculations point to the heterogeneity of acid sites due to different aluminium sites in zeolite lattice, and due to several probable locations of acid sites around aluminium atoms. The analysis of experimental IR and ¹H NMR spectra in combination with current calculations suggests that the experimentally observable mean acidity of zeolite ZSM-5 depends on temperature as the occupancies of protons at various oxygen sites are kinetically controlled and thermodynamic equilibrium is reached at high temperatures.

6. REFERENCES

1. R.J. Argauer, G.R. Landolt, US Patent 3702886, 1972.
2. H. van Bekkum, E.M. Flanigen, J.C. Jansen, (Eds.), Introduction to Zeolite Science and Practice, Studies in Surface Science and Catalysis, Vol. 58, Elsevier, Amsterdam, 1991.
3. V.L. Zholobenko, L.M. Kustov, V.Yu. Borovkov, V.B. Kazansky, Zeolites 8 (1988) 175.
4. J. Datka, B. Gil, P. Baran, Microporous and Mesoporous Materials 58 (2003) 291.
5. L.M. Kustov, Topics in Catal. 4 (1997) 131.
6. G.L. Woolery, L.B. Alemany, R.M. Dessau, A.W. Chester, Zeolites 14 (1986) 14.
7. E. Brunner, K. Beck, M. Koch, L. Heeribout, H.G. Karge, Microporous Mater. 3 (1995) 395.
8. L.B. Beck, J.L. White, J.F. Haw, J. Am. Chem. Soc. 116 (1994) 9657.
9. D. Freude, Chem. Phys. Lett. 235 (1995) 69.
10. F. Wakabayashi, J.N. Kondo, K. Domen, C. Hirose, J. Phys. Chem. 100 (1996) 1442.
11. J. Datka, B. Gil, P. Baran, B. Staudte, React. Kinet. Catal. Lett. 77 (2002) 209.
12. E. Brunner, J. Mol. Struct. 355 (1995) 61.
13. L. Heeribout, P. Batamack, C. Dorémieux-Morin, R. Vincent, J. Fraissard, Colloids Surfaces A: Physicochem. Eng. Aspects 115 (1996) 229.
14. L. Heeribout, C. Dorémieux-Morin, J.-P. Nogier, R. Vincent, J. Fraissard, Microporous and Mesoporous Materials 24 (1998) 101.
15. P. Sarv, C. Fernandez, J.-P. Amoureux, K. Keskinen, J. Phys. Chem. 100 (1996) 19223.
16. W. Zhang, X. Bao, X. Guo, X. Wang, Catal. Lett. 60 (1999) 89.
17. A.P. Kentgens, D. Iuga, M. Kalwei, H. Koller, J. Am. Chem. Soc. 123 (2001) 2925.
18. E. Brunner, J. Chem. Soc. Faraday. Trans. 86 (1990) 3957.
19. D. Freude, J. Klinowski, J. Chem. Soc. Chem. Comm. 1988 1411.
20. M. Hunger, D. Freude, H. Pfeifer, W. Schieger, Chem. Phys. Lett. 167 (1990) 21.
21. M. Hunger, D. Freude, D. Fenzke, H. Pfeifer, Chem. Phys. Lett. 191 (1992) 391.
22. T. Baba, N. Komatsu, Y. Ono, H. Sugisawa, J. Phys. Chem. B 102 (1998) 804.
23. H. Pfeifer. in: NMR Basic Principles and Progress, Vol. 31, P. Diehl, E. Fluck, H. Günther, R. Kosfeld, J. Seelig Eds. Springer-Verlag, Berlin, 1994, p. 31.
24. J. Sauer, M. Sierka, J. Comput. Chem. 21 (2000) 1470.
25. M. Brändle, J. Sauer, J. Am. Chem. Soc. 120 (1998) 1556.
26. U. Eichler, M.; Brändle, J. Sauer, J. Phys. Chem. B 101 (1997) 10035.
27. A.H. De Vries, P. Sherwood, S.J. Collins, A.M. Rigby, M. Rigutto, G.J. Kramer, J. Phys. Chem. B 103 (1999) 6133.
28. J. Sauer, P. Ugliengo, E. Garrone, V.R. Saunders, Chem. Rev. 94 (1994) 2095.
29. E.G. Derouane, J. Fripiat, Zeolites 5 (1985) 167.
30. H. V. Brand, L.A. Curtiss, L.E. Iton, J. Phys. Chem. 96 (1992) 7725.
31. H. V. Brand, L.A. Curtiss, L.E. Iton, J. Phys. Chem. 97 (1993) 12773.
32. K.-P. Schröder, J. Sauer, M. Leslie, C.R.A. Catlow, Zeolites 12 (1992) 20.
33. D. Nachtigallova, P. Nachtigall, M. Sierka, J. Sauer, Phys. Chem. Chem. Phys. 1 (1999) 2019.
34. R. Grau-Crespo, A.J.G.Peralta, A.R Ruiz-Salvador, A.I. Gomez, R. Lopez-Cordero, Phys. Chem. Chem. Phys. 2 (2000) 5716.

35. J. Dedecek, D. Kauchy, B. Wichterlova, O. Gonsiorova, *Phys. Chem. Chem. Phys.* 4 (2002) 5406.
36. V. Gabova, J. Dedecek, J. Cejka, *Chem. Commun.* (2003) 1196.
37. O.H. Han, C.-S. Kim, S.B. Hong, *Angew. Chem. Int. Ed.* 41 (2002) 469.
38. J.-R. Hill and J. Sauer. *J. Phys. Chem.* 98 (1994) 1238.
39. J.-R. Hill and J. Sauer. *J. Phys. Chem.* 99 (1995) 9536.
40. G. Ricchiardi, J.M. Newsam, *J. Phys. Chem. B* 101 (1997) 9943.
41. A.E. Alvarado-Swaisgood, M.K. Barr, P.J. Hay, A. Redondo, *J. Phys. Chem.* 95 (1991) 10031.
42. A. Redondo, P.J. Hay, *J. Phys. Chem.* 97 (1993) 11754.
43. G.S. Tschumper, K. Morokuma, *J. Mol. Struct. (Theochem)* 592 (2002) 137.
44. P.B. Karadakov, K. Morokuma, *Chem. Phys. Lett.* 317 (2000) 589.
45. I. Roggero, B. Civalleri, P. Ugliengo, *Chem. Phys. Lett.* 341 (2001) 625.
46. W. Panjan, J. Limtrakul, *J. Mol. Struct. (Theochem)* 654 (2003) 35.
47. K. Bobuatong, J. Limtrakul, *Appl. Catal. A* 253 (2003) 49.
48. X. Solans-Monfort, J. Bertran, V. Branchadell, M. Sodupe, *J. Phys. Chem. B* 106 (2002) 10220.
49. A. Damin, F. Bonino, G. Ricchiardi, S. Bordiga, A. Zecchina, G. Lamberti, *J. Phys. Chem. B* 106 (2002) 7524.
50. M. Svensson, S. Humbel, R.D.J. Froese, T. Matsubara, S. Sieber, K. Morokuma, *J. Phys. Chem.* 100 (1996) 19357.
51. S. Humbel, S. Sieber, K. Morokuma, *J. Chem. Phys.* 105 (1996) 1959.
52. S. Dapprich, I. Komaromi, K.S. Byun, K. Morokuma, M.J. Frisch, *J. Mol. Struct. (Theochem)* 461–462 (1999) 1.
53. E. Derat, J. Bouquant, S. Humbel, *J. Mol. Struct. (Theochem)* 632 (2003) 61.
54. Gaussian 98, Revision A.7, M.J. Frisch, G.W. Trucks, H.B. Schlegel, G.E. Scuseria, M.A. Robb, J.R. Cheeseman, V.G. Zakrzewski, J.A. Montgomery, Jr., R.E. Stratmann, J.C. Burant, S. Dapprich, J.M. Millam, A.D. Daniels, K.N. Kudin, M.C. Strain, O. Farkas, J. Tomasi, V. Barone, M. Cossi, R. Cammi, B. Mennucci, C. Pomelli, C. Adamo, S. Clifford, J. Ochterski, G.A. Petersson, P.Y. Ayala, Q. Cui, K. Morokuma, D.K. Malick, A.D. Rabuck, K. Raghavachari, J.B. Foresman, J. Cioslowski, J.V. Ortiz, A.G. Baboul, B.B. Stefanov, G. Liu, A. Liashenko, P. Piskorz, I. Komaromi, R. Gomperts, R.L. Martin, D.J. Fox, T. Keith, M.A. Al-Laham, C.Y. Peng, A. Nanayakkara, C. Gonzalez, M. Challacombe P.M. W. Gill, B. Johnson, W. Chen, M. W. Wong, J.L. Andres, C. Gonzalez, M. Head-Gordon, E.S. Replogle, and J.A. Pople, Gaussian, Inc., Pittsburgh PA, 1998.
55. H. van Koningsveld, *Acta Crystallogr. B* 34 (1990) 731.
56. M.J.S. Dwyer, W. Thiel, *J. Am. Chem. Soc.* 99 (1977) 4899.
57. J.A. Pople, A.P. Scott, M.W. Wong, L. Radom, *Isr. J. Chem.* 33 (1993) 345.
58. M. Sierka, U. Eichler, J. Datka, J. Sauer, *J. Phys. Chem. B* 102 (1998) 6367.
59. F. Haase, J. Sauer, *J. Am. Chem. Soc.* 117 (1995) 3780.
60. J.P. Chauvel Jr., N.S. True, *Chem. Phys.* 95 (1985) 435.
61. I.A. Koppel, P. Burk, I. Koppel, I. Leito, T. Sonoda, M. Mishima, *J. Am. Chem. Soc.* 124 (2000) 5114.
62. F. Jensen, *Introduction to Computational Chemistry*, John Wiley & Son Ltd, Chichester, 1999.
63. D. Freude, J. Klinowski, H. Hamdan, *Chem. Phys. Lett.* 149 (1988) 355.
64. N.P. Kenaston, A.T. Bell, J.A. Reimer, *J. Phys. Chem.* 98 (1994) 894.

65. J. Datka, M. Boczar, P. Rymarowicz, *J. Catal.* 144 (1988) 368.
66. M.A. Makarova, A.F. Ojo, K. Karim, M. Hunger, J. Dwyer, *J. Phys. Chem.* 98 (1994) 3619.
67. L.M. Kustov, V.B. Kazansky, S. Beran, L. Kubelkova, P. Jiru, *J. Phys. Chem.* 91 (1987) 5247.
68. M. Trombetta, T. Armadori, A.G. Alejandre, J.R. Solis, G. Busca, *Appl. Catal. A* 192 (2000) 125.
69. H. Knözinger, S. Huber, *J. Chem. Soc., Faraday Trans.* 94 (1998) 2047.
70. I.N. Senchenya, E. Garrone, P. Ugliengo, *J. Mol. Struct. (Theochem)* 386 (1996) 93.
71. K.J. Farnworth, P.J. O'Malley, *J. Phys. Chem.* 100 (1996) 1814.
72. M.V. Frash, M.A. Makarova, A.M. Rigby, *J. Phys. Chem. B* 101 (1997) 2116.
73. L.K. Kustov, V.Yu. Borovkov, V.B. Kazansky, *J. Catal.* 72 (1981) 149.
74. E. Garrone, V.B. Kazansky, L.K. Kustov, J. Sauer, I.N. Senchenya, P. Ugliengo, *J. Phys. Chem.* 96 (1992) 1040.
75. B. Civalieri, E. Garrone, P. Ugliengo, *J. Phys. Chem. B* 102 (1998) 2373.
76. H. Mix, J. Sauer, K.-P. Schröder, A. Merkel, *Coll. Czech. Chem. Commun.*, 53 (1988) 2191.
77. J. Sauer, U. Eichler, U. Meier, A. Schäfer, M. von Arnim, R. Ahlrichs, *Chem. Phys. Lett.*, 308 (1999) 147.
78. J.L. White, L.W. Beck, J.F. Haw, *J. Am. Chem. Soc.* 114 (1992) 6182.
79. A. Chatterjee, D. Bhattacharya, M. Chatterjee, T. Iwasaki, *Microporous Mesoporous Mater.* 32 (1999) 189.
80. T. Demuth, J. Hafner, L. Benco, H. Toulhoat, *J. Phys. Chem. B* 104 (2000) 4593.
81. E.L. Meijer, R.A. van Santen, A.P.J. Jansen, *J. Phys. Chem. A* 103 (1999) 2553.
82. S. Bates, J. Dwyer, *Chem. Phys. Lett.* 255 (1994) 427.
83. S.S. Stave, J.B. Nicholas, *J. Phys. Chem.* 99 (1995) 15046.
84. H. Koller, E.L. Meijer, R.A. van Santen, *Solid State NMR* 9 (1997) 165.
85. H. Koller, G. Engelhardt, R.A. van Santen, *Topics in Catalysis* 9 (1999) 163.
86. P. Sarv, T. Tuherm, E. Lippmaa, K. Keskinen, A. Root, *J. Phys. Chem.* 99 (1995) 13763.
87. M. Sierka, J. Sauer, *J. Phys. Chem. B* 105 (2001) 1603.

SUMMARY IN ESTONIAN

Tseoliit ZSM-5 happelisuse tsentrite teoreetiline uurimus

Tseoliidid on mikropoorsed kristalsed alumosilikaadid. Antud töös käsitletud tseoliit ZSM-5 on tugev tahke hape ning on seetõttu leidnud kasutust katalüsaatorina naftakeemiatööstuses. Tseoliitide katalüütiline aktiivsus tuleneb tseoliidis olevatest Brønstedi happelisuse tsentritest, milleks on nn sildmised hüdroksüülrühmad (Si-O(H)-Al). Katalüütiliste protsesside paremaks tundmiseks on oluline teada nende hüdroksüülrühmade asukohta ning jaotust tseoliidi kristallvõres, nende happelisuse tsentrite struktuuri ja tugevust.

Ekspérimentaalselt on laialt levinud sildmiste hüdroksüülrühmade uurimine IP- ja TMR-spektroskoopia meetoditega. Detailsemat informatsiooni aktiivsete tsentrite kohta on võimalik saada kasutades kvantkeemia meetodeid. Ekspérimentaalselt määratud suuruste täpseks kvantkeemiliseks modelleerimiseks peab kasutama kõrgetasemelisi arvutusmeetodeid (st kasutama suuri baase ning elektronkorrelatsiooni arvestavaid meetodeid), millega aga tseoliitide puhul, arvestades uuritavate süsteemide suurust, kaasnevad kitsendused vastavate arvutuste teostamisel.

Käesolevas väitekirjas on tseoliit ZSM-5 happelisuse tsentrite modelleerimiseks kasutatud ONIOM meetodit. ONIOM meetod on mõeldud suurte molekulaarsete süsteemide arvutamiseks — suured süsteemid jagatakse kihtideks, kus keemiliselt tähtsa osa (näiteks reaktsioonitsentri) arvutamiseks kasutatakse kõrgetasemelist arvutusmeetodit, ülejäänud osa molekulist käsitletakse aga madalamal arvutuslikul tasemel.

Töö esimeses osas katsetati mitmeid ONIOM meetodi kombinatsioone, leidmaks parimat lähendust tseoliit ZSM-5 happelisuse tsentrite arvutuslikuks modelleerimiseks. Näidati, et kasutades ONIOM meetodit on võimalik kirjeldada erinevates kristallvõre sõlmedes paiknevate sildmiste hüdroksüülrühmade karakteristikuid.

Töö teises osas kasutati ONIOM meetodit tseoliit ZSM-5 kristallvõre erinevates asukohtades olevate aktiivsete tsentrite struktuuride ning energeetiliste ja spektroskoopiliste omaduste uurimiseks. Leiti, et tseoliit ZSM-5 kristallvõres olevad sildmised hüdroksüülrühmad võivad moodustada vesiniksideme mõne naabruses oleva võre hapnikuaatomiga st moodustuvad nn teist tüüpi happelisuse tsentrid. Arvutuste tulemused näitavad happelisuse tsentrite heterogeenset paiknemist tseoliit ZSM-5 kristallvõres. Sellele viitavad vähemalt kahe võimaliku mitteekvivalentse alumiiniumiaatomi asukoha olemasolu ning mitme tõenäolise protoneerimistsentri eksisteerimine mõlema alumiiniumiaatomi ümber. Lähtuvalt eksperimendaalsete IP- ja ^1H TMR-spektrite analüüsist ning antud töös teostatud arvutustest leiti, et happelisuse tsentrite asukoht, tüüp ja tugevus tseoliit ZSM-5 kristallvõres sõltub temperatuurist ja seega on ka uuritud tseoliidi üldine (keskmine) happelisuus sõltuv temperatuurist.

ACKNOWLEDGMENTS

I wish to express my greatest gratitude to my supervisor Professor Peeter Burk for his great guidance, time and energy.

I would like to thank all my friends and all the people in Department of Chemistry for being a great model and making my studies here most enjoyable.

I am deeply grateful to my family for their firm and undoubtful support.

The financial support of this research by Estonian Science Foundation (through grants 3361 and 5196) is gratefully acknowledged.

PUBLICATIONS

CURRICULUM VITAE

Kaido Sillar

Born: December 14, 1975, Tallinn, Estonia
Citizenship: Estonian
Marital status: single
Address: Institute of Chemical Physics,
University of Tartu,
2 Jakobi St., Tartu 51014, Estonia
Phone: +372 7 375 258
Fax: +372 7 375 264
E-mail: ksillar@ut.ee

Education

1994–1998 University of Tartu, Department of Chemistry, *B.Sc.*
(chemistry) 1998
1998–2000 University of Tartu, Department of Chemistry, *M.Sc.*
(chemistry) 2000
2000–present University of Tartu, Department of Chemistry, *Ph.D.*
student, doctoral advisor prof. Peeter Burk

Professional employment and retraining

2002–2003 University of Tartu, Centre of Strategical Competence, researcher
2003– University of Tartu, Institute of Chemical Physics, chemist

Main scientific publications

1. P. Burk, K. Sillar, Acidity Of Saturated Hydrocarbons, *J. Mol. Struct. (Theochem)*, 535 (2001) 49–59.
2. P. Burk, K. Sillar, I.A. Koppel, Gas-Phase Basicities and Proton Affinities of Alkali Metal Oxides and Hydroxides. A Theoretical Study, *J. Mol. Struct. (Theochem)*, 543 (2001) 223–231.
3. K. Sillar, P. Burk, Calculation of the Properties of Acid Sites of the Zeolite ZSM-5 Using ONIOM Method, *J. Mol. Struct. (Theochem)*, 589–590 (2002) 281.

4. K. Sillar, P. Burk, Hybrid Quantum Chemical and Density Functional Theory (ONIOM) Study of the Acid Sites in Zeolite ZSM-5, *J. Phys. Chem. B*, 108 (2004) 9893.
5. K. Sillar, P. Burk. Computational Study of Vibrational Frequencies of Bridging Hydroxyl Groups in Zeolite ZSM-5, *Chem. Phys. Lett.* 393 (2004) 285.

ELULOOKIRJELDUS

Kaido Sillar

Sündinud: 14. detsember 1975, Tallinn, Eesti
Kodakondsus: Eesti
Perekonnaseis: vallaline
Aadress: Keemilise füüsika instituut, Tartu Ülikool,
Jakobi 2, 51014 Tartu, Eesti
Tel: +372 7 375 258
Faks: +372 7 375 264
E-mail: ksillar@ut.ee

Haridus

1994–1998 Tartu Ülikooli keemiaosakonna üliõpilane, *B.Sc.* (keemia) 1998
1998–2000 Tartu Ülikooli keemiaosakonna magistrant, *M.Sc.* (keemia) 2000
2000– Tartu Ülikooli keemiaosakonna doktorant, juhendaja prof.
Peeter Burk

Teenistuskäik

2002–2003 Tartu Ülikool, Tehnoloogiakeskus, erakorraline teadur
2003– Tartu Ülikool, Keemilise füüsika instituut, keemik

Tähtsamad teaduspublikatsioonid

1. P. Burk, K. Sillar, Acidity Of Saturated Hydrocarbons, *J. Mol. Struct. (Theochem)*, 535 (2001) 49–59.
2. P. Burk, K. Sillar, I.A. Koppel, Gas-Phase Basicities and Proton Affinities of Alkali Metal Oxides and Hydroxides. A Theoretical Study, *J. Mol. Struct. (Theochem)*, 543 (2001) 223–231.
3. K. Sillar, P. Burk, Calculation of the Properties of Acid Sites of the Zeolite ZSM-5 Using ONIOM Method, *J. Mol. Struct. (Theochem)*, 589–590 (2002) 281.
4. K. Sillar, P. Burk, Hybrid Quantum Chemical and Density Functional Theory (ONIOM) Study of the Acid Sites in Zeolite ZSM-5, *J. Phys. Chem. B*, 108 (2004) 9893.
5. K. Sillar, P. Burk. Computational Study of Vibrational Frequencies of Bridging Hydroxyl Groups in Zeolite ZSM-5, *Chem. Phys. Lett.* 393 (2004) 285.